24th EUROPEAN ROTORCRAFT FORUM
Marseille, France - 15th -17th September 1998

Reference: AC 10

Noise Reduction of Fenestrons Using Integrated Helmholtz Resonators

O. Recker; G. Neuwerth
Lehrstuhl für Luft- und Raumfahrt, Prof. Dr.-Ing. D. Jacob
Rheinisch-Westfälische Technische Hochschule Aachen, Germany

Abstract

Compared to a conventional tail rotor the remarkable features of a fenestron are the increased efficiency as well as the operational safety and the reduced noise emission. An uneven rotor blade spacing and an optimised stator positioning contribute to the low noise level of the original fenestron. This paper demonstrates the potential of reducing the noise even further by installing Helmholtz Resonators into the fenestron shroud. Two different types of Helmholtz-Resonators were used. Type 1 consists of a large number of small resonators with one orifice per volume. Type 2 consists of one ring-like volume with only four partitions and nearly 600 orifices. Such a resonator can be built with low weight and cost penalties. The noise reduction of these resonators was investigated experimentally and theoretically. For the experiments a 1:1.4 wind-tunnel model of the Eurocopter EC 135 fenestron was built with two different rotor heads (7 equally spaced rotor blades; 7 unevenly spaced rotor blades), 11 stator blades and a removable ring, which allows the integration of different resonators. The preliminary design of the resonator geometry was made using the empirical model of Hersh/Walker. The design was improved by measurements using the two microphone method, which take the influence of high sound pressure level and grazing flow into account. An optimised resonator was then integrated into the fenestron shroud. Wind-tunnel tests showed, that the sound power level of single frequencies could be reduced more than 6 dB.

Nomenclature

Symbol	Unit	Description
a_i	-	Ratio of Two Volume Flow Rates
c	m/s	Speed of Sound
d	m	Diameter of Orifice Aperture
e	m	Length of a Side of a Square Resonator Cavity
f	Hz	Frequency
h	m	Depth of Resonator Cavity
k	1/m	Wave-number
l_o	m	Orifice Thickness
m_0	kg/m^2	Fluctuating Mass per Unit Orifice Area
n_{Rotor}	1/min	Rotor Rotation per Minute (rpm)
p	$kg/(ms^2)$	Pressure
p_i	$kg/(ms^2)$	Sound Pressure of Incoming Sound
$\underline{p}_{cav}$	$kg/(ms^2)$	Sound Pressure of Resonator Cavity
$\underline{p}_{sound}$	$kg/(ms^2)$	Sound Pressure of Orifice Aperture
t	s	Time
v	m/s	Forward Flight Velocity
$\underline{v}$	m/s	Speed of Air
v_{ax}	m/s	Axial Flow Velocity Through the Fenestron
$\underline{v}_o$	m/s	Speed of Air in Orifice Aperture
$\underline{v}_{cav}$	m/s	Speed of Air in Resonator Cavity
x	m	x co-ordinate
x_{Wall}	m	Distance From the Cavity Bottom in x-Direction
y	m	y co-ordinate
B_{Rotor}	-	Number of Rotor Blade
BPF	Hz	Blade Passing Frequency
C_o	m	Upper Area Border
C_u	m	Lower Area Border
D	m	Diameter of Round Resonator Cavity
J_1	-	Bessel Function of 1.Order
P_{Loss}	Watt	Power Loss of Resonator
R	$kg/(m^2s)$	Resistance in Orifice Aperture
R	m	Distance Between Two Sources
S_1	-	Struwe Function of 1.Order
S_{ori}	m^2	Orifice Area
T	-	Transfer Function
Z	$kg/(m^2s)$	Specific Sound Resistance
Z_{ori}	$kg/(m^2s)$	Orifice Impedance of Helmholtz Resonator
φ	rad	Phase Angle
ρ	kg/m^3	Density of Air
σ	-	Orifice-to-Resonator Cavity Open

		Area Ratio (Porosity)
ω	1/s	Angular Frequency
θ	°	Angle of Incidence
ϕ	rad	Phase Angle
o		Index for Ambient Conditions
+		Index for Incoming
-		Index for Reflected
^		Diacritic for Amplitude

1. Introduction

The paper describes the first results of a research project on the reduction of fenestron noise, which started at the Lehrstuhl für Luft- und Raumfahrt at the University of Technology Aachen (RWTH), Germany in 1996 in co-operation with Eurocopter Germany. The research was financed by the Bundesministerium für Bildung, Wissenschaft Forschung und Technologie.

Previous research work of Eurocopter concentrated on direct measures to reduce the noise penetration of the fenestron of the EC 135 helicopter. Mainly the unequally spaced rotor blades and the non-radial positioning of the stator blades led to a reduced overall A-weighted sound pressure level [1]. The research project described here deals with additional indirect measures of noise reduction, which aim at a decrease of noise already created. Compared to conventional tail rotors fenestrons have the advantage that their shroud can be utilised for the integration of sound absorbing devices. Due to the tonal spectrum of fenestron noise, Helmholtz resonators with their resonance frequency tuned to the frequency of interest are suitable to absorb the emitted noise.

2. Preliminary Considerations

Before integrating Helmholtz Resonators into a fenestron shroud, the space for integrating these resonators must be exactly specified. Figure 2.1 shows a cross section of the fenestron model, which was built during this research project (detailed description in chapter 2.1).

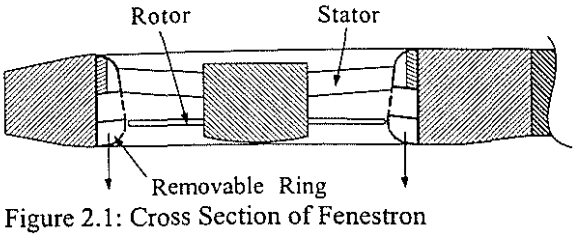

Figure 2.1: Cross Section of Fenestron

To allow different resonator configurations to be investigated a removable ring around the rotor and stator plane was constructed. Unfortunately not the whole surface of this ring can be used for integrating Helmholtz Resonators, because a large amount of thrust is produced by the inlet in front of the rotor plane. The available space for resonator integration is shown in Figure 2.2.

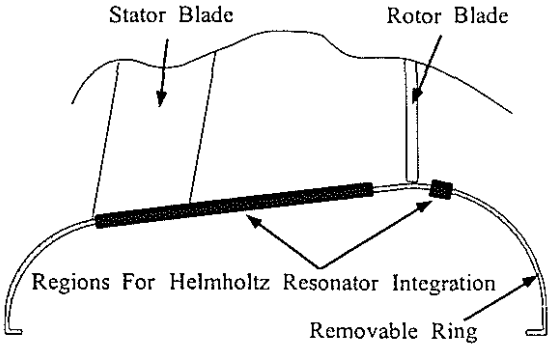

Figure 2.2: Available Space for Resonator Integration

2.1 Test Facility

A model of the EC 135 fenestron (scale 1:1.4) was built using two different rotor heads: one with 7 equally spaced rotor blades, the other with 7 unevenly spaced rotor blades. The number of stator blades was 11. The rotational speed was set to 3584 rpm, which is identical with the original fenestron rpm. The fenestron is mounted to the test facility, which drives the rotor electrically by a belt drive. A picture of this test facility showing the fenestron model in the wind-tunnel of the institute is presented in Figure 2.3. The removable ring surrounding the rotor plane can also be recognised in this Figure.

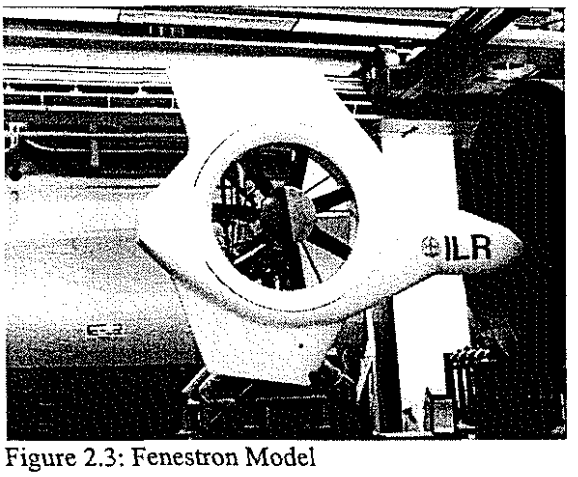

Figure 2.3: Fenestron Model

The absorption of the integrated resonators is influenced by the flow through the fenestron. Therefore the model must have the same velocity and pressure distribution as the original. The velocity distributions depend on the flight speed of the helicopter so that five different flight cases with varying forward flight speed from 0 - 40 m/s were defined. The velocity distribution was measured using hot wire anemometry, while the pressure distribution on the fenestron shroud was measured with pressure orifices. The results of these measurements are shown in Figure 2.4.

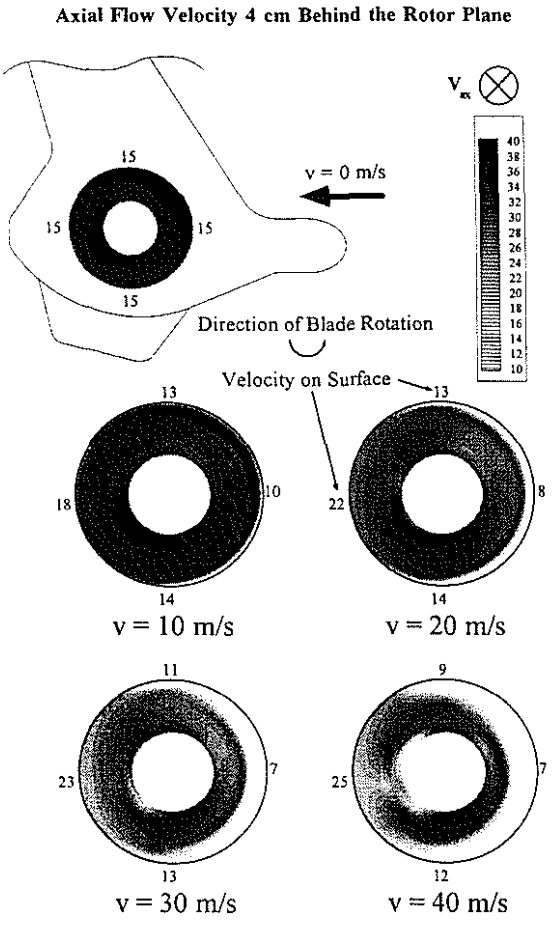

Figure 2.4: Velocity Distribution 4 cm Behind the Rotor Plane

From the velocity distribution in Figure 2.4 follows Figure 2.5, where the original fenestron thrust and the model thrust are plotted taking the scale of the model into consideration.

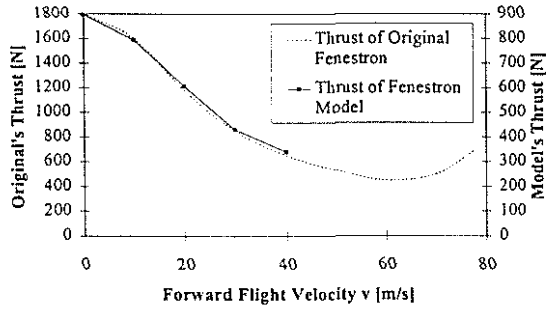

Figure 2.5 Comparison Between the Thrust of the Original And the Model Fenestron

To define the noise emission without absorbing devices the sound power level of the fenestron model was measured with the help of a rotating microphone in the wind-tunnel room, which acts as a reverberatory chamber. The result for the forward flight velocity v = 0 m/s and a rotor head with 7 equally spaced blades is presented in Figure 2.6.

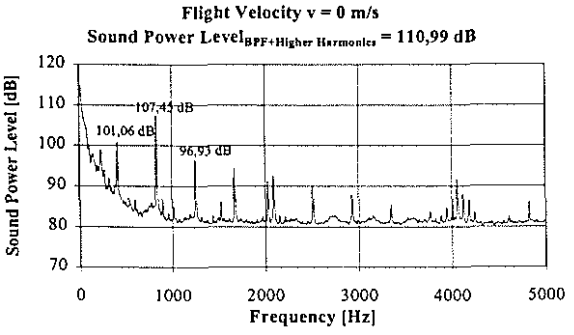

Figure 2.6: Sound Power Spectrum of the Fenestron Model without Absorbing Devices

The largest sound power level was found at the blade passing frequency (BPF=418 Hz) and the first two harmonics (836 Hz and 1254 Hz), so it was decided to absorb noise at these frequencies.

3. Designing Procedure

In Figure 3.1 a typical Helmholtz Resonator is shown.

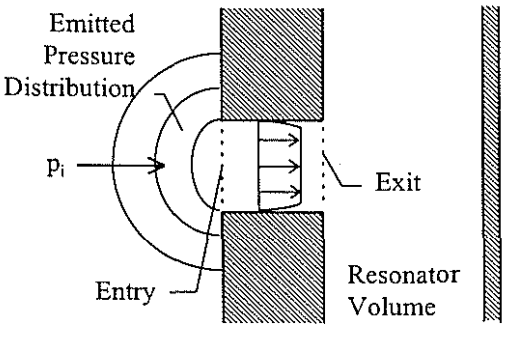

Figure 3.1: Helmholtz Resonator

All definitions of the quantities used in the following equations can be found in the nomenclature.

To describe the sound absorption of this Helmholtz Resonator the power loss in the resonator orifice is used:

$$P_{Loss} = \tfrac{1}{2}|v_{ori}|^2 Z_{Drag} S = 2\frac{|p_i|^2 S_{ori} Z_{Drag}}{|Z_{ori}|^2} \qquad (3.1)$$

The power loss in a resonator orifice depends on the sound particle velocity in the orifice, the drag in the orifice and the orifice area. Taking into consideration that the area for integrating Helmholtz Resonators in the fenestron is limited, a definition of power loss per area is introduced. The area e^2 is the internal cross-section of the resonator. It follows:

$$\frac{P_{Loss}}{e^2} = 2\frac{|p_i|^2 \sigma Z_{Drag}}{|Z_{ori}|^2} \qquad (3.2)$$

The unknown parameter Z_{ori} can be determined by the forces, which drive the mass flow inside the orifice. These forces are due to the incoming pressure, the mass inertia, the drag on the orifice surface and the pressure at the orifice exit. As a consequence the impedance of the orifice is the sum of the entry impedance, the inertial impedance, the flow resistance and the exit impedance. It follows:

$$\frac{P_{Loss}}{e^2} = 2\frac{|p_i|^2 \sigma Z_{Drag}}{\left|Z_{Entry} + Z_{MassInertia} + Z_{Drag} + Z_{Exit}\right|^2} \qquad (3.3)$$

The drag impedance is a real number, while the impedance due to mass inertia and the exit impedance are only imaginary numbers (complete explanation follows in chapter 3.3 and 3.5). As a consequence P_{Loss}/e^2 has a maximum when all imaginary parts of the equation become zero and the real parts of Z_{Entry} equals the real part of Z_{Drag} (Figure 3.2).

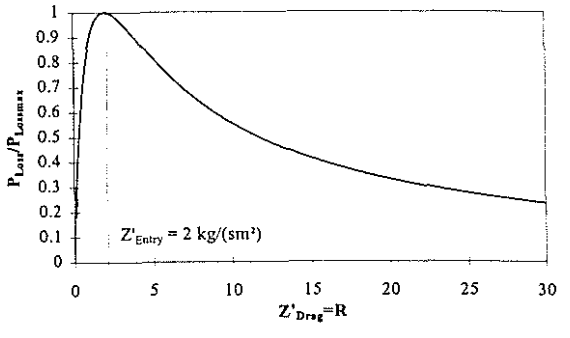

Figure 3.2: Dependence of $P_{Loss}/P_{Lossmax}$ on Z'_{Drag}

In the following subchapters determinations of the influencing parameters p_i, σ, Z_{Entry}, $Z_{MassInertia}$, Z_{Drag} and Z_{Exit} are described.

3.1 Measuring the Incident Sound Pressure p_i

By installing microphones into the fenestron surface the sound pressure distribution on the fenestron shroud was measured. For hover the measured sound pressure on the fenestron model surface can be seen in Figure 3.3.

The sound pressure distribution on the fenestron surface is not only important for the calculations of the power loss. It has also a large influence on the absorption of a Helmholtz Resonator.

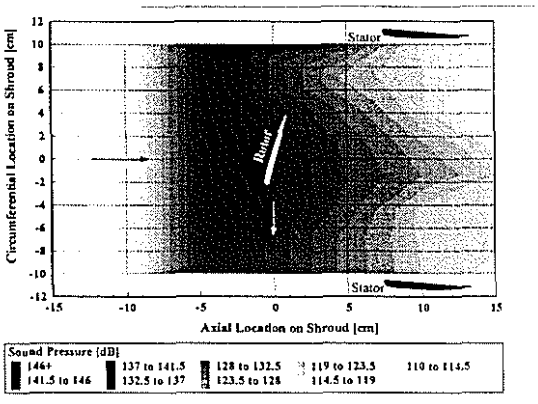

Figure 3.3: Sound Pressure Distribution of the First Harmonic on the Fenestron Shroud for Hover

3.2 Calculation of the Entry Impedance

The entry impedance Z_{Entry} of a Helmholtz Resonator can be described by the radiation impedance of a piston radiator located on a plane surface. The following assumptions are made to solve the complete equation for the entry impedance.

i. The sound particle velocity is constant over the entire orifice area. The assumption is good enough for use in the Helmholtz Resonator equation. The actual velocity profile depends on the orifice diameter and the frequency of sound. The accuracy of the assumption improves with increasing diameter or increasing frequency.
ii. Only a plane wave exists inside the orifice.
iii. The diameter of the orifice is very small compared to the wavelength of the incidence sound.

With the co-ordinate system given in figure 3.4 the complete equation is as follows [2]:

$$\frac{Z_{Entry}}{Z_0} = \frac{i}{2\pi}\iint_{k_0^2 A}\frac{e^{-jk_0R}}{R}d\left(k_0^2 A\right)$$

$$= \frac{i}{2\pi}\int_{k_0x_u}^{k_0x_o} d(k_0x_0)\int_{k_0C_u(x_0)}^{k_0C_o(x_0)}\frac{e^{-ik_0R}}{k_0R}d(k_0y_0)$$

$$= \frac{1}{2\pi}\int_{k_0x_u}^{k_0x_o} d(k_0x_0)\int_{k_0C_u(x_0)}^{k_0C_o(x_0)}\left[\frac{\sin k_0R}{k_0R} + i\frac{\cos k_0R}{k_0R}\right]d(k_0y_0) \qquad (3.4)$$

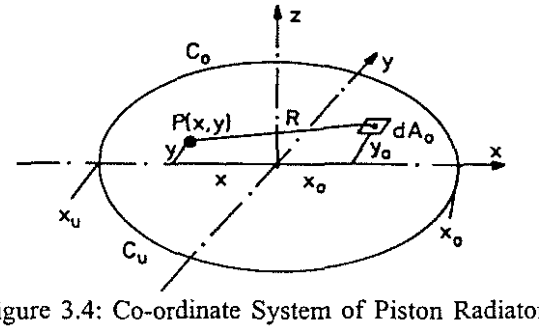

Figure 3.4: Co-ordinate System of Piston Radiator Used in Equation 3.4 [2]

And the solution to Equation (3.4) is:

$$\frac{Z_{entry}}{\rho_0 c_0} = 1 - \frac{J_1(k_0 d)}{k_0\, d/2} + j\frac{S_1(k_0 d)}{k_0\, d/2} \qquad (3.5)$$

If there are several resonators the flow field of one resonator influences the other because the piston radiator has to work against the pressure field of the other piston radiators. A complete derivation of this influence can be found in /1/. Here only the result is presented:

$$Z_{Entry} = Z'_{Entry,0}\left[1 + \sum_{i=1}^{N} a_i \left(\frac{\sin(k_0 x_i + \varphi_0 - \varphi_i)}{k_0 x_i} + i\frac{\cos(k_0 x_i + \varphi_0 - \varphi_i)}{k_0 x_i}\right)\right] + iZ''_{Entry,0} \qquad (3.6)$$

So the entry impedance of Helmholtz Resonators influencing each other depends on the entry impedance $Z'_{Entry,0}$ of a resonator without neighbouring orifices, the number N of influencing resonators, the ratio a_i of the volume flow rate of the influencing resonator to the volume flow rate of the influenced resonator, the wave number k of the sound, the distance x between the resonators and the phase difference φ_0-φ_i between the sound emission of the resonators.

A program was written to compute Z'_{Entry} according to equation 3.6, taking the measured sound pressure level on the surface and a phase distribution as estimated in Figure 3.5 into consideration. Three different distances between the orifices and different orifice diameters were calculated. For an orifice diameter of 13 mm and a distance x between the orifices of x = 35 mm (see Figure 3.6) the entry resistance follows as shown in table 3.1.

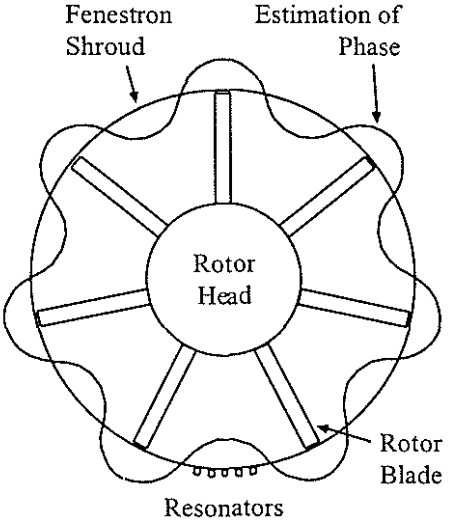

Figure 3.5: Estimated Phase Distribution on Shroud

The imaginary component $Z''_{Entry,0}$ of the entry impedance can be neglected in the optimisation process. For values of $\frac{d}{x} < 0.5$, the entry reactance can easily be made zero along with all the other imaginary parts in the denominator of the power loss equation (see equation 3.3).

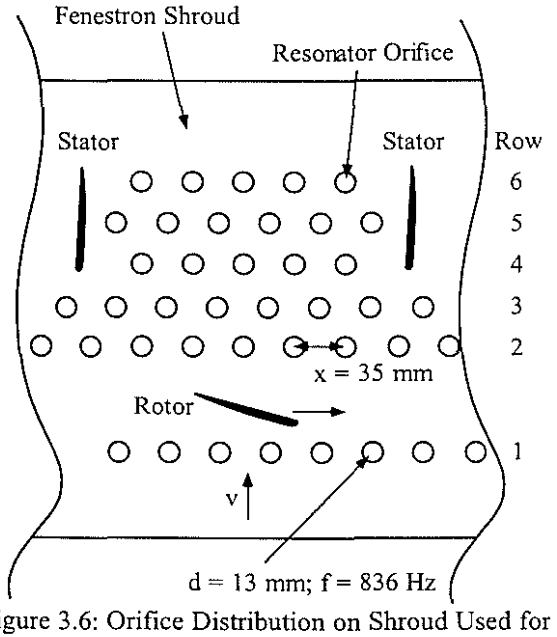

Figure 3.6: Orifice Distribution on Shroud Used for Calculations

Row	Z'_{Entry} [kg/(s m²)]
1	1.77
2	2.76
3	3.54
4	5.00
5	9.81
6	23.04

Table 3.1: Entry Resistance

3.3 Derivation of the Inertial Impedance of a Helmholtz Resonator

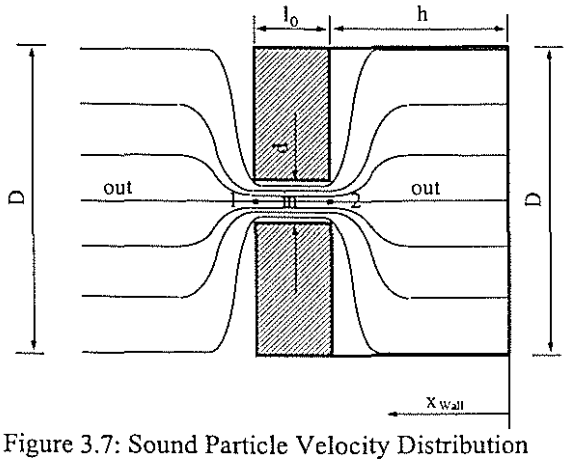

Figure 3.7: Sound Particle Velocity Distribution

Applying the equation of continuity through the orifice aperture gives:

$$v_{out}\frac{\pi D^2}{4} = v_{in}\frac{\pi d^2}{4} \tag{3.7}$$

The ratio of aperture area to the base area of the resonator cavity is given by:

$$\sigma = \left.\frac{d^2}{D^2}\right|_{round} \hat{=} \left.\frac{\pi d^2}{4e^2}\right|_{square} = \frac{v_{out}}{v_{in}} \tag{3.8}$$

Applying the Euler equation inside the aperture between point 1 and point 2, the following result is obtained:

$$-\frac{\partial \underline{p}}{\partial x} = \rho\frac{\partial \underline{v}_{in}}{\partial t} \tag{3.9}$$

$$LHS = -\frac{\partial \underline{p}}{\partial x} = -\frac{\Delta \underline{p}}{\Delta x} = \frac{\underline{p}_1 - \underline{p}_2}{l_0} \tag{3.10}$$

$$RHS = \rho\frac{\partial \underline{v}_{in}}{\partial t} = i\omega\rho\underline{v}_{in} = i\omega\rho\frac{\underline{v}_{out}}{\sigma} \tag{3.11}$$

The surface density, i.e., the mass per unit area is defined as:

$$m_0 = \frac{\rho l_0}{\sigma} \tag{3.12}$$

Thus the inertial component of impedance is given by the following equation.

$$\underline{Z}_{MassInertia} = \frac{\underline{p}_1 - \underline{p}_2}{\underline{v}_{out}} = \frac{i\omega\rho l_0}{\sigma} = i\omega m_0 \tag{3.13}$$

An end correction is required for both sides of the orifice aperture since the flow does not come to a sudden halt at the opening end of the aperture.

$$m = m_0 + 2\Delta m = \frac{\rho}{\sigma}\left(l_0 + \frac{\pi}{4}d\right) \tag{3.14}$$

3.4 Measuring the Flow Resistance of Helmholtz Resonators

Though it is possible to calculate the drag inside a resonator orifice with the help of the 1-D Navier Stokes equation, the results of these calculations are not exact and they do not take into consideration the influence of high sound pressure levels or a grazing flow. Therefore the drag was measured with a small wind-tunnel and an experimental set-up as described in Figure 3.8.

Using the two microphone method shown in Figure 3.8 the transfer function between the microphones can be used to determine the drag of the resonator as a function of the frequency with the following equation:

$$Z_{Drag} = R = \frac{-\sigma\rho c\sin\phi}{|\underline{T}_{12}|\sin\left(\frac{\omega h}{c}\right)} \tag{3.15}$$

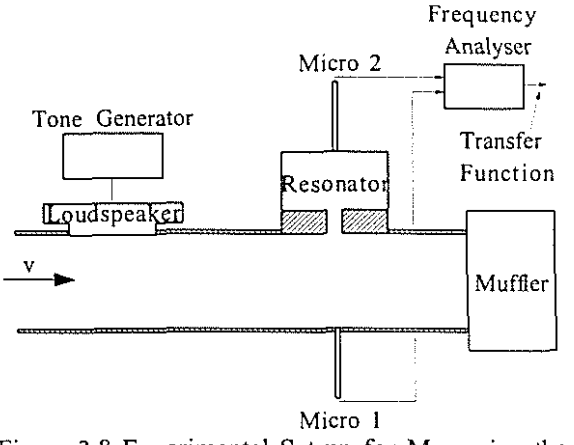

Figure 3.8 Experimental Set-up for Measuring the Flow Resistance

Measurements were made changing the orifice diameter from 4 - 22 mm. For every diameter six different cavities were built to vary the porosity from 4% to 30%. The result of this measurement is shown in Figure 3.9

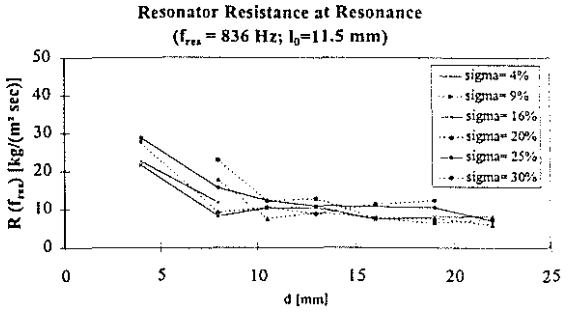

Figure 3.9 Measured Resonator Resistance

The measurements in Figure 3.9 were made with a sound pressure level identical to the level on the fenestron shroud but without grazing flow. The influence of a grazing flow on the drag depends on the velocity of the flow and the angle of incidence An increasing or decreasing drag is possible. Even negative drag values leading to sound production occur at certain velocities or angels of incidence [3, 4, 6]. The resonance frequency of the system also depends on the flow speed because of the change in the fluctuating mass. Therefore the usual Helmholtz Resonator cannot be used to conditions with grazing flow.

In Figure 2.4 the grazing flow velocity on the fenestron shroud was already presented. For hover a velocity of 15 m/s was measured, but the values given in Figure 2.4 are time averaged data. An example for the actual axial velocity in hover near the fenestron shroud is shown in Figure 3.10. It can be seen that the velocity fluctuates between 5 m/s and 35 m/s with an average value of 15 m/s. Therefore a resonator, which creates a constant drag for a velocity range from 0 - 40 m/s, has to be designed.

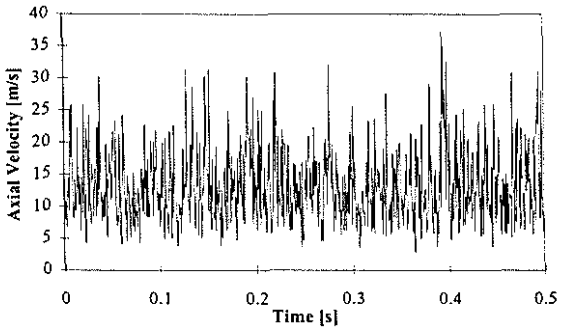

Figure 3.10: Axial Velocity on the Shroud in Hover

The influence of a grazing flow can be reduced by several devices, for example membranes covering the orifice to separate the flow in the resonator orifice from the grazing flow. However, these membranes increase the fluctuating mass considerably and their behaviour depends on the membrane's tension, which cannot be kept constant for a large number of orifices and a long period of time. So in our case grids were used to separate the outer flow from the orifice flow (see Figure 3.11).
Several different grids were tested with wire thicknesses from 0.2 mm to 0.5 mm and mesh widths from 0.3 mm to 1.8 mm. All grids increase the drag due to their presence in the orifice flow. Usually this leads to a decrease in power loss, because the orifice drag is larger than the entry resistance (see Figure 3.2).
For a velocity range from 0 to 40 m/s a grid with a wire thickness of 0.3 mm and a mesh width of 0.5 mm (grid C) produced a drag nearly independent of the velocity of the outer flow. It turned out to be the best compromise between reducing the influence of grazing flow and increasing the resistance. The measured resistances including grid C are plotted in Figure 3.12. The increased resistance compared to Figure 3.9 can clearly be seen.

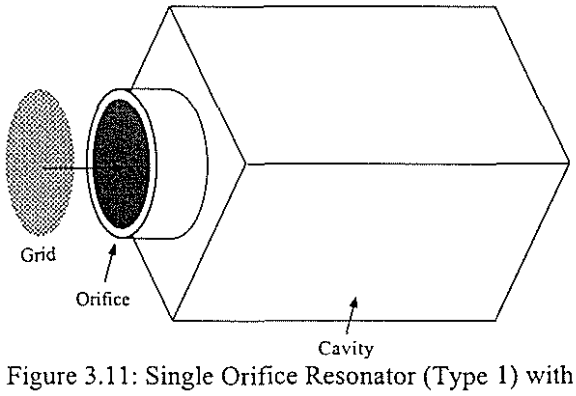

Figure 3.11: Single Orifice Resonator (Type 1) with Grid

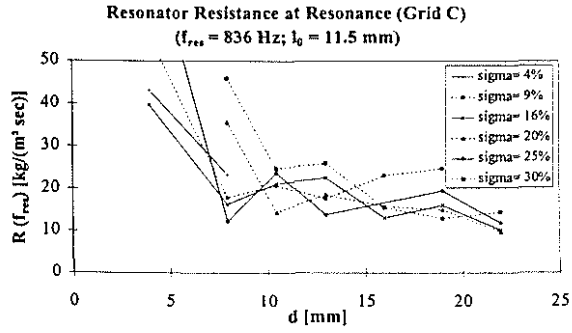

Figure 3.12 Measured Resonator Resistance (Grid C)

3.5 Derivation of the Exit Impedance of A Helmholtz Resonator

The exit impedance Z_{Exit} follows from the pressure and velocity distribution in front of the wall behind the orifice (see figure 3.7). Assuming that all the sound is reflected and the wave propagation can be described by a plane wave, the velocity and pressure are:

$$\underline{v}_2 = \underline{v}_{2+}e^{-ikx_{wall}} + \underline{v}_{2-}e^{ikx_{wall}} \quad (3.16)$$

$$\underline{p}_2 = \underline{p}_{2+}e^{-ikx_{wall}} + \underline{p}_{2-}e^{ikx_{wall}} \quad (3.17)$$

With the boundary condition, $\underline{v}_2(x_{Wall} = 0) = 0$

The exit impedance is given by the ratio $\frac{\underline{p}_2}{\underline{v}_2}$ at position $x_{wall} = h$:

$$\underline{Z}_{Exit} = \frac{\underline{p}_2}{\underline{v}_2} = \frac{\underline{p}_{2+}}{\underline{v}_{2+}} \frac{e^{-ikh} + e^{ikh}}{e^{-ikh} - e^{ikh}} = \rho c \coth(ikh) \quad (3.18)$$

$$\coth(ikh) = -i\cot(kh) \quad (3.19)$$

$$\underline{Z}_{Exit} = -i\rho c \cot(kh) = -i\rho c \cot\left(\frac{\omega h}{c}\right) \quad (3.20)$$

The assumption that the wave propagation can be described by the plane wave theory is only correct for single orifice resonators as shown in Figure 3.11. If a volume has got several orifices the exit impedance is not only dependent on the cavity depth (equation 3.20) but also on the cavity width and the incoming sound pressure. Figure 3.13 illustrates the influence.
In Figure 3.13 two sound pressures approach a resonator with one volume but two orifices. If the two sound pressures are identical in amplitude and phase the sound particle velocity in y-direction equals to zero inside the cavity at the dotted line and the assumption of plane wave propagation in x-direction is correct. In any other case mass is moving across the dotted line so that there is a wave propagation in y-direction. This propagation influences the exit impedance of the orifice. Measurements showed that a small difference in phase has only a small influence on the exit

impedance, whereas different amplitudes have a large effect on the exit impedance. Looking at the sound pressure distribution on the fenestron shroud (Figure 3.3) in hover a sound pressure difference only occurs perpendicular to the rotor plane. Here the circumferential sound pressure distribution is also estimated as constant in forward flight. Therefore the walls separating a volume perpendicular to the rotor plane can be left away. This decreases the cost and weight penalties of integrating resonators. Figure 3.14 shows the two different types of resonators.

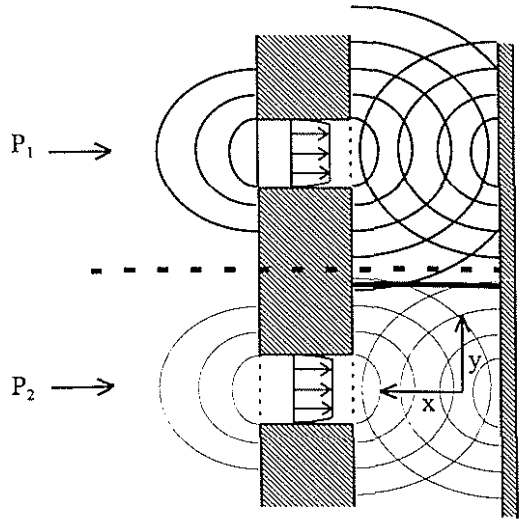

$$\underline{p}_1 = \hat{p}_1 \cdot e^{i(\omega t+\varphi_1)}$$

$$\underline{p}_2 = \hat{p}_2 \cdot e^{i(\omega t+\varphi_2)}$$

$$\hat{p}_1 \neq \hat{p}_2$$

Figure 3.13: Resonator with Several Orifices per Volume (Type 2)

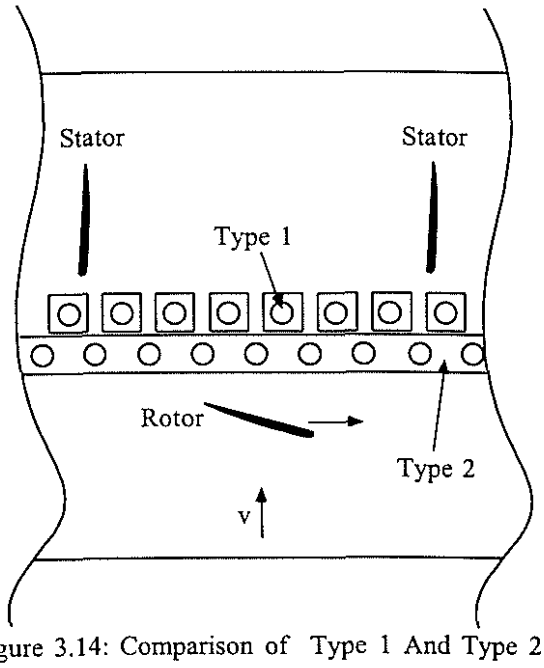

Figure 3.14: Comparison of Type 1 And Type 2 Resonators

3.6 Solving the Power Loss Equation

Despite the availability of exact equations for all parameters influencing the power loss equation, empirical solutions are very popular. The reason is the existence of discrepancies between predictions by the exact equations and measurements. These discrepancies are large concerning the resistances in the power loss equation, whereas the reactances are calculated quiet exactly. The reason for the large discrepancies in the resistance terms is that the exact equations do not represent the reality correct enough for high sound pressure levels or grazing flow effects.

Consequently empirical parameters have to be added for a better correlation of measurements with predictions. The empirical solution in this research project is that of Hersh/Walker. A detailed explanation of their model can be found in [5,6] and will not be presented here. For solving the power loss equation it is only important to know that the impedance due to mass inertia and the exit impedance were calculated using this model. All imaginary parts of the power loss equation could be made to zero using this model. As described in chapter 3.4 the drag in the orifice was measured for several different resonator geometries, while the entry resistance was calculated using the piston radiator model (chapter 3.2). The result of this modelling and measuring on the power loss equation (equation 3.3) is shown graphically in Figure 3.15

Figure 3.15 shows that the maximum power loss is achieved for a diameter of 16 mm (l_0 = 11.5 mm) and a porosity σ of 30%. It can be seen that the maximum power loss for other large values of σ is generally close to a diameter of 16mm.

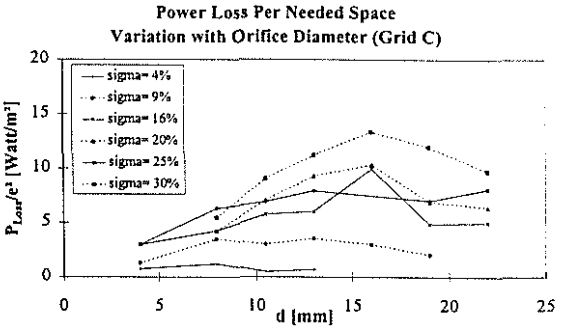

Figure 3.15 Graphical Presentation of the Results of Solving the Power Loss Equation (Equation 3.3) with Grid C

4. Wind-Tunnel Measurements

Unfortunately the size of the cavity needed for a diameter of 16 mm and σ = 30% is too large (e = 26 mm) to be integrated in front of the rotor plane. So for wind-tunnel testing a diameter of 13 mm, σ = 30% and e = 21 mm was chosen. In addition to the limitation of space in front of the rotor plane the length available inside the model for

the orifice and the cavity is limited to 75 mm (see Figure 4.6). Using a diameter of 13 mm and σ = 30% the length limitation leads to a resonator, which can absorb noise in a frequency range from 600Hz - 1800 Hz. Thus to reduce the noise of the blade passing frequency (418 Hz) a diameter of 7 mm (l_0= 22 mm; e = 21 mm) was installed.

4.1 Integrating Type 1 Resonators

The size of the cavities allowed the integration of 345 resonators. A technical drawing of the a resonator with 13 mm orifice diameter is presented in Figure 4.1.

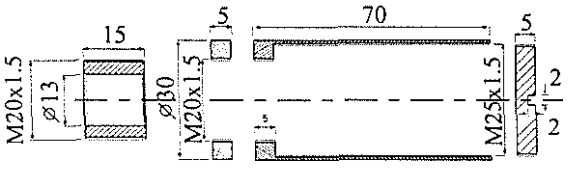

Figure 4.1: Cross Section of Optimum Resonator

Because of financial constraints a simplified resonator had to be designed. It consists of square sections of aluminium material for the resonator cavities and of round fuse fixation rings of 13 mm diameter, length 10.5 mm for the orifice. This far cheaper arrangement (see figure 4.2) shows the disadvantage that the cavity depth can no longer be changed, when the acrylic glass plate is glued into the aluminium cross section, whereas the resonator design in figure 4.1 allows a changing of the cavity depth by a thread. So differences between the resonator behaviour in the wind-tunnel measurements and in the fenestron model could not be corrected.

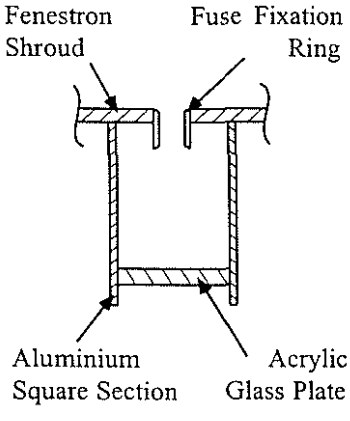

Figure 4.2: Cross Section of Installed Resonator

The positions of the orifices were drilled in the surface of a removable ring located around the rotor and stator so that the distance between every orifice is 35 mm in the end. Figure 4.3 shows the distribution of the orifices and the corresponding tuned resonance frequencies. Figure 4.4 presents the integrated resonators.

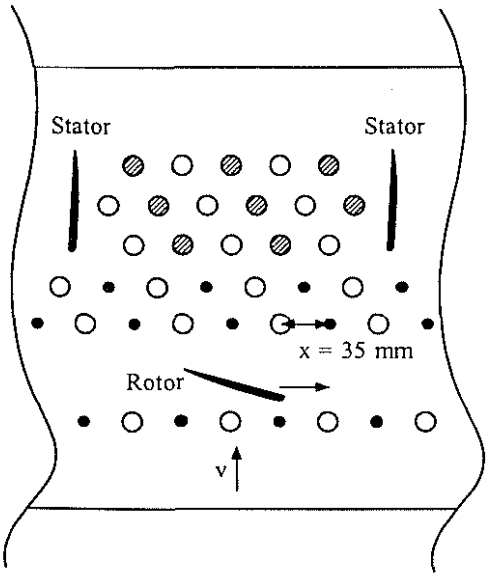

● d = 7 mm; l_0 = 22 mm; h = 64 mm; f = 418 Hz

○ d = 13 mm; l_0 = 10.5 mm; h = 59 mm; f = 836 Hz

◍ d = 13 mm; l_0 = 10.5 mm; h = 29 mm; f = 1254 Hz

Figure 4.3: Orifice Distribution on Shroud

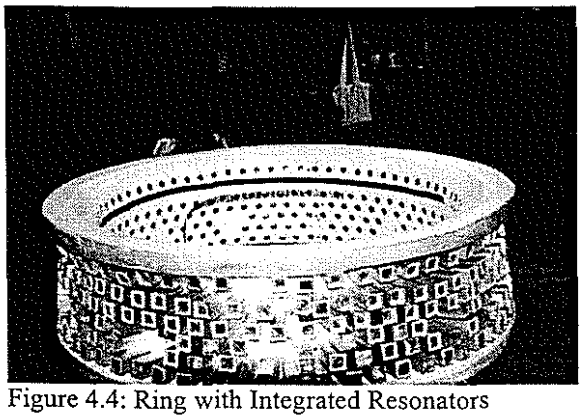

Figure 4.4: Ring with Integrated Resonators

4.2 Integrating Type 2 Resonators

Type 2 resonators are much easier to install because of their ring-like volume (see figure 3.14). To reduce the expenditures of labour further more only the holes in the shroud surface should represent the resonator orifice. The resonators were tuned only to the blade passing frequency and the first harmonic. The orifice diameter was set to 10.5 mm for the blade passing frequency and 7 mm for the first harmonic, whereas the orifice depth was given by the thickness of the fenestron shroud (l_0 = 1.5 mm). This arrangement is presented in Figure 4.5.

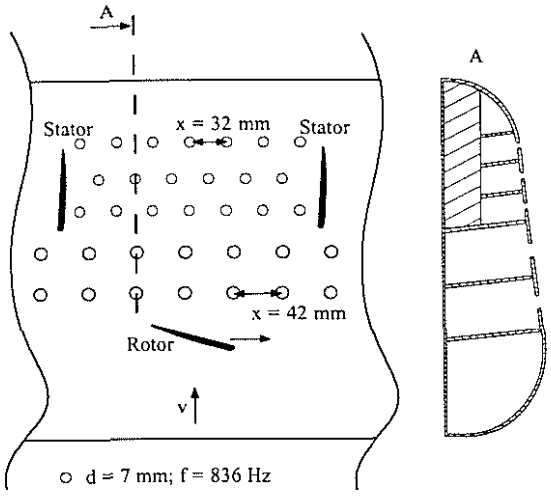

Figure 4.5

4.3 Apparatus Set-up

Figure 4.6 shows the fenestron model in the wind-tunnel fitted with Helmholtz Resonators mounted on a pylon structure. For the first campaign an equal blade spacing has been applied.

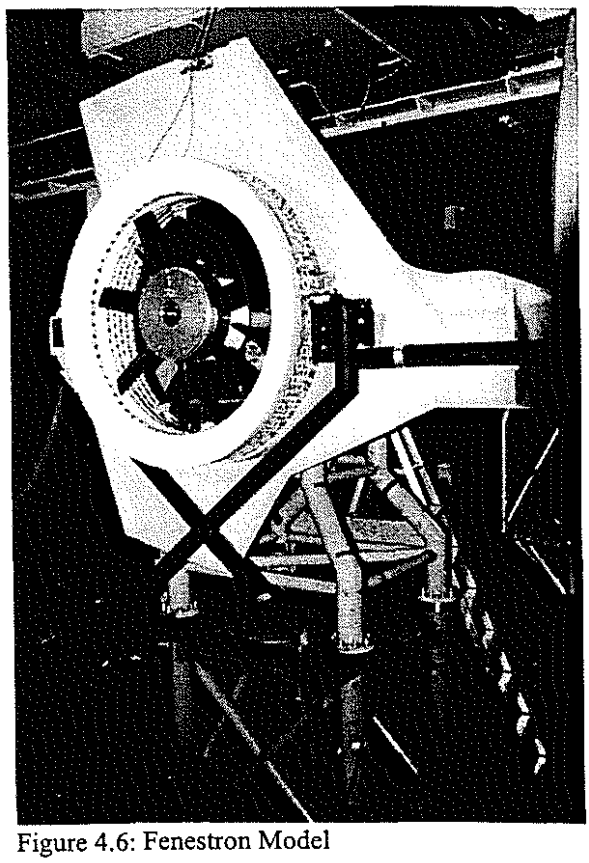

Figure 4.6: Fenestron Model

The model contains provisions to use the two microphone method. These provisions can be found at four different circumferential positions. One microphone is placed close to the orifice and the second at the bottom of the resonator. This enabled to measure the sound pressure on the surface of the fenestron and the transfer function between the microphone on the shroud and the microphone in a cavity. Both were displayed by a frequency analyser during the measurements.

The sound power level of the fenestron was measured with the help of a rotating microphone in the wind tunnel room, which acts as a reverberatory chamber.

4.4 Measurement Results

For each flight case three measurements were carried out to have reproducible results. The results without the resonators fitted into the fenestron were used for comparison.

In the first measurements a large increase in the sound power level of the higher harmonics was found out. This increase disappeared, when the resonator row in front of the rotor plane was covered with tape. From this it can be seen that the orifice flow disturbs the flow, which approaches the rotor blades. These disturbances create unsteady blade forces leading to an increase of rotor sound emission. Therefore during the following measurements the resonators in front of the rotor plane were kept covered. The measured reduction in sound power level for type 1 and type 2 resonators are given in Figure 4.7 and 4.8.

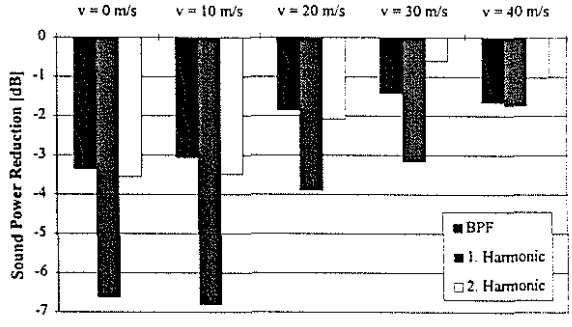

Figure 4.7: Measured Noise Reduction Using Type 1 Resonators

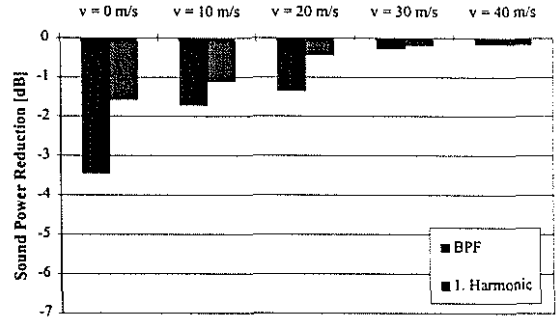

Figure 4.8: Measured Noise Reduction Using Type 2 Resonators

The figures show that for type 1 resonators a better result was achieved. The main reason for that is that in type 1 resonators no circumferential sound propagation, which tunes the resonators to different

resonance frequencies, is possible. In addition no grids were used for type 2 resonators.
The results for type 1 resonators are very good. The 1. Harmonic, which was absorbed by nearly 50% of all resonators, could be reduced more than 6 dB. The reduction of the sound power level of the blade passing frequency and the 2. Harmonic was less, because less resonators were tuned to these frequencies. The largest reduction could be achieved in hover and for a forward flight velocity of 10 m/s. For larger velocities the reduction decreases. The reason for that can be found in the flow through the fenestron. Transfer function measurements of resonators, whose orifices are directed in forward flight direction, indicate, that the flow blows into these resonators. This reduces the resonators ability to absorb noise.
From the transfer function measurements it could also be seen that not all resonators were tuned to the correct frequency. In addition the measurements of the resonator row, which is placed directly behind the rotor plane, showed that the wake of the rotor blows into the resonator. The location of these resonators was set too close to the rotor plane. Therefore especially the position of the resonators on the fenestron shroud can be improved.

5. Application of the Model Results to the Original Fenestron

The original fenestron has 10 unevenly spaced rotor blades. As a consequence the frequency of the emitted noise is different compared to the model fenestron. In Figure 5.1 the emitted noise of a EC 135 helicopter during landing is plotted. The landing condition is chosen, because in this flight condition the fenestron emits the highest noise level.

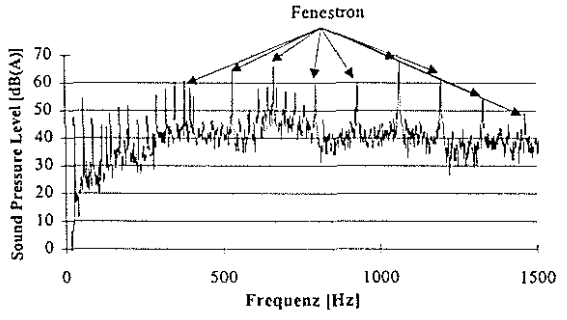

Figure 5.1: Spectrum of the Original Fenestron During Landing

Figure 5.1 shows that during landing the fenestron creates the highest peaks in the A-weighted spectrum. These peaks are at 532 Hz, 665Hz and 1064 Hz. With the design of the optimum resonator (d = 16 mm, σ = 30%), it is possible to absorb noise of every frequency between 300Hz and 1800 Hz by just changing the cavity depth (using two different orifice depths). Then the frequencies of the emitted noise of the original fenestron do not create any absorption problems.
The velocity distribution on the original fenestron does not differ from the model as explained earlier. Leaving the rotational speed constant while scaling down to 1:1.4 leads to a lower tip Mach number at the model. Consequently the emitted noise of the original fenestron increases and higher sound pressure levels on the fenestron shroud can be expected. These increased sound pressure levels lead to a change in the resonator impedance. The resistance rises due to non linear jetting effects at the orifice [5, 7, 8] and the reactance decreases because of less fluctuating mass inside the orifice. The change in the resonators reactance can be compensated by changing the cavity depth, whereas the higher resistance leads to lower power loss in the orifice.
Because of it's larger size more resonators can be integrated into the original fenestron, which increases the power loss. In addition it is possible to install the optimum resonator (d = 16mm) into the original fenestron, while in the model only the less effective resonator with a diameter of 13 mm was used.
The measurements and these arguments show, that the noise of the original fenestron will also be reduced by approximately the same amount as achieved in the fenestron model.

6. Conclusions And Objectives for the Future

This research project deals with the reduction of fenestron noise using Helmholtz Resonators. With the help of the power loss per area an equation for the absorption of Helmholtz Resonators in a lattice structure was derived. An optimum resonator was designed for the absorption at high sound pressure levels including the influence of a grazing flow. This resonator with an orifice diameter of 16 mm, an orifice depth of 11.5 mm and a porosity of 30% turned out to be too large for an integration in a 1:1.4 fenestron model, which was built for wind-tunnel testing. Therefore a modified resonator of 13 mm orifice diameter was installed into the fenestron shroud. With the help of resonators single tones of the fenestron spectrum could be reduced more than 6 dB. This shows that Helmholtz Resonators are well suited to reduce the noise of fenestrons. It can be expected that these results also apply to the original fenestron.
The measurements with the uneven rotor blade spacing have just begun. The obtained results show that the same good absorption can be achieved.
Integrating single orifice resonators (type 1), which showed a higher absorption compared to the resonators with a ring-like volume (type 2), is still bound up with high cost and weight penalties. An easier way to integrate these resonators must be achieved. Preliminary consideration concerning this

problem led to the installation of honeycomb structures for resonator cavity design.
The realisation of Helmholtz Resonators as a component, which can be integrated into the fenestron with low structural and cost demands, is the most important objective for the future.

Literature

[1] Niesl, G. and Arnaud, G.: Low Noise Design of the EC 135 Helicopter Presented at the American Helicopter Society 52nd Annual Forum, Washington D.C., June 4-6, 1996

[2] Mechel, F.P.: Schallabsorber, Hirzel Verlag, 1989

[3] Baumeister, K.J. and Rice, E.J.: Visual Study of the Effect of Grazing Flow on the Oscillatory Flow in a Resonator Orifice, NASA TM X-3288, 1975

[4] Phillips, B.: Effects of High Wave Amplitude and Mean Flow on a Helmholtz Resonator, NASA-TM-X-1582, 1968

[5] Hersh, A.S. and Walker, B.E.: Acoustic Behaviour of Helmholtz Resonators: Part I. Non-linear Model, CEAS/AIAA-95-078

[6] Hersh, A.S. and Walker, B.E.: Acoustic Behaviour of Helmholtz Resonators: Part II. Effects of Grazing Flow, CEAS/AIAA-95-079

[7] Ingard, U.: On the Theory and Design of Acoustic Resonators, J. Acoust. Soc. Am., Vol 25, No. 6, 1953, p 1037-1061

[8] Ingard, U., Ising, H.: Acoustic Nonlinearity of an Orifice, J. Acoust. Soc. Am., Vol. 42, No. 1, 1967, p 6-17